Macromolecules

pubs.acs.org/Macromolecules Article

# Temperature Dependence of Chain Conformations and Fibril Formation in Solutions of Poly(*N*-isopropylacrylamide)-Grafted Methylcellulose

McKenzie L. Coughlin, Jerrick Edmund, Frank S. Bates,* and Timothy P. Lodge*

Cite This: *Macromolecules* 2022, 55, 550−558 Read Online

ACCESS | Metrics & More | Article Recommendations | Supporting Information

**ABSTRACT:** As a water-soluble cellulose ether, methylcellulose (MC) is used in a variety of applications that take advantage of its thermoreversible gelation. Recent work has shown that MC gelation is due to the formation of nanofibrils with a relatively uniform diameter (*ca.* 15 nm) and that gelation and fibril formation can be suppressed through the addition of low-molecular-weight poly(ethylene glycol) as grafts along the backbone. In this work, we modify MC similarly with thiol-terminated poly(*N*-isopropylacrylamide) (PNIPAm, $M_w \approx 3$ kg/mol) using thiol−ene click chemistry and investigate the resulting influence on aqueous MC solution properties. From static and dynamic light scattering, it is apparent that the coil dimensions increase with grafting density (up to 0.11 grafts/anhydroglucose repeat unit), which leads to an increase in the persistence length inferred from the Kratky−Porod wormlike chain model. The data are consistent with a model based on the incorporation of graft−graft and graft−backbone excluded volume interactions. Interestingly, grafting PNIPAm leads to an increase in the theta temperature, even though PNIPAm typically has a lower critical solution temperature (LCST) that is lower than bare MC. Small-angle X-ray scattering and cryogenic transmission electron microscopy reveal that fibril formation still occurs at high temperature for the grafted chains.

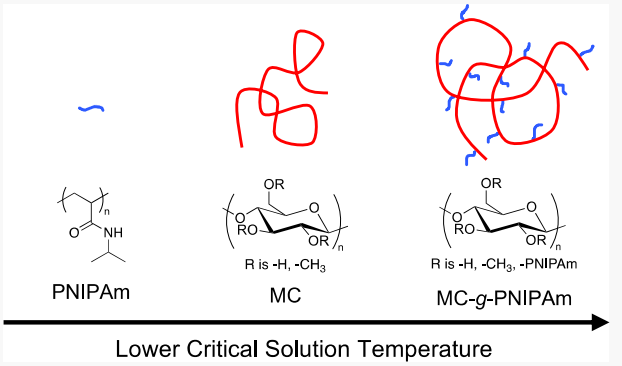




## INTRODUCTION

Methylcellulose (MC) is a water-soluble cellulose ether used in applications ranging from pharmaceuticals and food to personal care products and construction materials, typically as a viscosity modifier or binder.[1,2] It has been known for decades that aqueous MC solutions gel thermoreversibly upon heating above the lower critical solution temperature (LCST) around 60 °C when the average degree of substitution is about 1.8−2.0 methoxy groups per anhydroglucose repeat unit.[3−14] This gelation behavior has been attributed to the formation of nanofibrils of relatively uniform radius (*ca.* 7−8 nm),[14−20] a value that has been shown to be largely independent of MC molecular weight, concentration, and temperature of formation.[14−17] Recent efforts have focused on understanding the mechanism of fibril formation and the underlying cause of the surprisingly invariant fibril radius. Schmidt et al.[18] showed that the fibrils are semicrystalline in nature, with the chain backbone predominantly oriented along the fibril axis, and Liberman et al.[21] indirectly confirmed that the amorphous regions are swollen with water; the addition of salt modifies the fibril radius. Morozova et al.[22,23] looked at the chemical modification of MC, making use of the unsubstituted hydroxyl groups along the chain. By sequential substitution of allyl groups and UV-initiated thiol−ene click chemistry, it was shown that low-molecular-weight thiol-terminated poly(ethylene glycol) (PEG) chains can be conjugated to MC at various grafting densities along the backbone. This modification systematically increased the persistence length of the polymers as a function of grafting density.[22] At low grafting densities, the fibril diameter increased as the number of PEG side chains increased, while fibril formation and gelation were suppressed at higher densities.[23] This result was reproduced in simulations by Sethuraman and Dorfman,[24] which showed that for high grafting density, the nucleating structures that lead to fibril formation are disrupted, preventing fibril formation upon heating. Morozova et al.[23] also showed that the transition from fibrils to aggregates in solution occurred at lower grafting density when the molecular weight of the PEG was increased. This method of attaching low-molecular-weight polymers to MC has opened potential avenues for modifying MC properties for expanded applications.

**Received:** October 23, 2021
**Revised:** December 28, 2021
**Published:** January 10, 2022

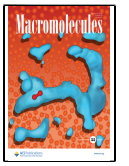





https://doi.org/10.1021/acs.macromol.1c02206
*Macromolecules* 2022, 55, 550−558

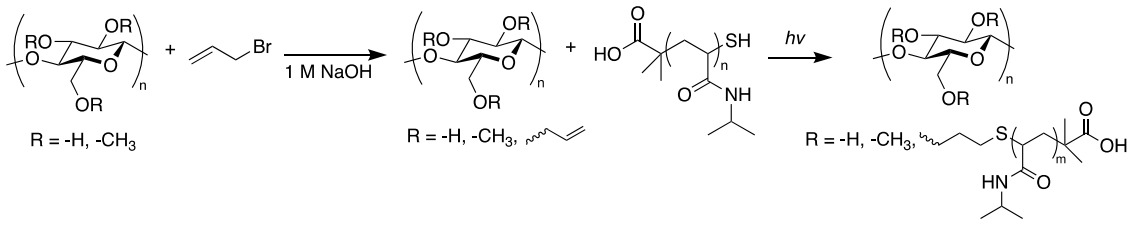


**Figure 1.** Thiol−ene grafting reaction scheme to synthesize PNIPAm-grafted MC.

Alternative methods of grafting polymers onto MC and other cellulose derivatives have been explored previously.[25−30] A particular graft of interest is poly(*N*-isopropylacrylamide) (PNIPAm), a water-soluble polymer that phase-separates and can gel upon heating.[31−39] The LCST is typically close to body temperature (*ca.* 37 °C), which makes it attractive for a variety of pharmaceutical applications. Previous work on attaching PNIPAm to cellulose-based polymers typically involved polymerizing NIPAm from MC or other cellulosics (*i.e.*, "grafting-from"), although the focus has primarily been on forming hydrogels with PNIPAm as the major component.[40−44] Addition of PNIPAm to MC has the potential to modify the thermal characteristics of the aqueous solution due to the difference in LCST behavior of the two polymers. For example, Liu et al.[42] used a grafting-from method to attach PNIPAm to 12 kg/mol MC and showed that the LCST of PNIPAm can be increased through the incorporation of MC. The authors focused on characterizing the PNIPAm properties; thus, it is not known if fibril formation still occurred for the PNIPAm-grafted MC.

In this work, we exploit the grafting-to chemistry developed by Morozova et al.[22,23] and focus on understanding how MC solution properties change with the incorporation of small amounts of PNIPAm. A series of PNIPAm-grafted MC polymers are synthesized, and the chain conformations are studied using light scattering as a function of graft density and temperature. The presence of fibrils at elevated temperature is confirmed by small-angle X-ray scattering (SAXS) and cryogenic transmission electron microscopy. These findings provide insight into how the chemistry of the graft affects MC self-assembly.

## MATERIALS AND METHODS

**Materials.** Methylcellulose (MC, $M_w \approx 150$ kg/mol, $Đ \approx 3.6$, degree of methoxy substitution DS = 1.8) was generously provided by the Dow Chemical Company. All other reagents including allyl bromide, IRGACURE D-2959 photoinitiator, and thiol-terminated poly(*N*-isopropylacrylamide) (PNIPAm-SH, $M_w \approx 3$ kg/mol, $Đ \approx 1.2$) were purchased from Sigma-Aldrich. To remove excess water, MC was dried under vacuum (∼100 mTorr) for 24 h at 50 °C. Allyl bromide and IRGACURE D-2959 were used without further purification. To purify the PNIPAm-SH, the solid was dissolved in water, filtered through a 0.45 μm Pall Acrodisc GHP syringe filter, dialyzed overnight using 0.5−1.0 kD MWCO dialysis tubing (SpectraPor Biotech Cellulose Ester (CE)), and lyophilized overnight to isolate the purified polymer. MC and MC-*g*-PNIPAm solutions were prepared by directly dissolving freeze-dried polymer into Millipore-filtered water. The solutions were stored in a refrigerator at 2 °C for at least 24 h before experiments.

**Chemical Modification.** Synthesis of PNIPAm-grafted MC was performed using thiol−ene click chemistry following a previously reported procedure[22,23] illustrated in Figure 1. Briefly, MC was first dissolved in 1 M NaOH with allyl bromide and reacted at room temperature overnight. The amount of allylation was controlled by changing the molar ratio of the MC monomer to allyl bromide. The solution was then neutralized with 1 M HCl and dialyzed in water overnight using 25 kD MWCO dialysis tubing (SpectraPor 6 Standard RC Pre-Wetted). The resulting allyl-MC was then recovered through freeze-drying. The amount of allylation ($\sigma_{allyl}$), defined as the average number of allyl groups per MC repeat unit, was quantified by $^1$H nuclear magnetic resonance (NMR) spectroscopic analysis in $D_2O$ using a Bruker Advance III HD 400 spectrometer with a 60-slot SampleXpress autosampler (Figure S1). The allylation resulted in allylated-MC with $\sigma_{allyl} = 0.014−0.16$. Here, we note that the amount of allylation is reaction-time-dependent and the reaction does not go to completion during the *ca.* 16 h at room temperature employed for the synthesis.

In the second step, allyl-MC was dissolved in water with 3 times molar excess of PNIPAm-SH and ∼0.05 mg IRGACURE D-2959 and allowed to react under UV light (295−360 nm) for 1−2 h. The unreacted PNIPAm-SH was removed through dialysis against water for 3−4 weeks using 25 kD MWCO dialysis tubing, and the purified MC-*g*-PNIPAm was recovered through freeze-drying. The grafting density ($\sigma$), defined as the average number of PNIPAm grafts per MC repeat unit, was determined using $^1$H NMR spectroscopy (Figure S2). Examination of the alkene region in the $^1$H NMR spectrum showed that essentially all allyl groups were consumed during the reaction. This synthesis strategy resulted in copolymers with $\sigma = 0.007−0.11$. Further discussion of the reaction procedures is provided in the Supporting Information.

**Light Scattering.** Static light scattering (SLS) experiments were performed on a Brookhaven BI-200SM instrument with a 10 mW laser for a $q = (4\pi n/\lambda_0)\sin(\theta/2)$ range of $6.79−22.7 \times 10^6$ m$^{-1}$, where $q$ is the magnitude of the scattering vector, $n$ is the refractive index of water (1.333), $\lambda_0$ is the laser wavelength in vacuum (637 nm), and $\theta$ is the scattering angle (30−120°). Samples were prepared by dissolving 2 mg/mL MC-*g*-PNIPAm in water. Six milliliter solutions of various concentrations were made by dilution of the 2 mg/mL stock solution and filtered through 0.45 μm Pall Acrodisc GHP syringe filters into clean 20 mL scintillation vials. The samples were stored in a refrigerator at 2 °C between measurements and held at the designated temperature (23−55 °C) for 30 min before each measurement. The Rayleigh ratio ($R_\theta$) of the sample was calibrated using a toluene standard, with $R_{\theta,toluene} = 9.5 \times 10^{-6}$ cm$^{-1}$ at 23 °C.[45] The refractive index increment ($\partial n/\partial c$) in water was 0.136 mL/g for MC and 0.167 mL/g for PNIPAm. For the grafted polymers, $\partial n/\partial c$ was calculated from the relative mass fractions of the backbone and grafts from NMR.

Dynamic light scattering (DLS) measurements were conducted on the same instrument with a Brookhaven BI-9000AT correlator and a 20 mW laser power for a $q$ range of $1.11−2.38 \times 10^7$ m$^{-1}$ (50−130°). The normalized intensity autocorrelation function ($g_2(t)$) was measured for 5−10 min at five angles for each sample. The 1 mg/mL samples prepared for SLS were used in DLS and were annealed for 30 min at the desired temperature prior to measurement. The measured $g_2(t)$ at each angle was converted to the electric field autocorrelation function ($g_1(t)$) using the Siegert relation[46] $g_2(t) = A(1 + B|g_1(t)|^2)$, where $A$ is the baseline and $B$ is the coherence factor. The data were then fit to a second-order cumulant expansion, where $g_1(t) = \exp(-\bar{\Gamma}t)(1 + \mu_2 t^2/2 + ...)$, to obtain the average decay rate ($\bar{\Gamma}$) and the dispersity ($\mu_2/\bar{\Gamma}^2$). The mutual diffusion coefficient ($D_m$) was estimated by taking the slope of $\bar{\Gamma}$ versus $q^2$ with zero intercept. For dilute solutions, $D_m$ can be used as an approximation for the tracer diffusion coefficient ($D_t$) to calculate the hydrodynamic radius


https://doi.org/10.1021/acs.macromol.1c02206
Macromolecules 2022, 55, 550−558

($R_h$) using the Stokes–Einstein equation[47] $R_h = k_B T/6\pi\eta_s D_t$, where $k_B$ is the Boltzmann constant, $T$ is the temperature, and $\eta_s$ is the temperature-dependent solvent viscosity. Additional analysis of the polymer size distribution was performed by applying the REPES Laplace inversion to the intensity autocorrelation function.[48] This algorithm results in a decay rate distribution ($G(\Gamma)$), which can be converted to the distribution of $R_h$ (Figure S3) to confirm monomodal distributions of polymer size.

**Small-Angle X-ray Scattering (SAXS).** SAXS experiments were performed at the Advanced Photon Source at Argonne National Laboratory, Sector 5-ID-D beamline of the Dupont-Northwestern-Dow Collaborative Access Team (DND-CAT). Solutions (0.75 mg/mL) of MC and MC-*g*-PNIPAm with $\sigma$ = 0.03 were prepared and placed in 1.5 mm diameter quartz capillary tubes sealed with epoxy. Samples were stored in a refrigerator at 2 °C between measurements and held at the designated temperature for 30 min on a custom-fabricated eight-capillary heating stage before each measurement. Two-dimensional (2D) scattering patterns were collected using a Rayonix MX170-HS detector with a 1 s exposure time, an X-ray wavelength of $\lambda$ = 0.0729 nm, and an 8.5 m sample-to-detector distance, giving a $q$ range of 2.35 × $10^{-3}$–0.137 $Å^{-1}$. To optimize the signal and decrease noise, the detector readout was binned to 4 by 4 pixels. The 2D data were averaged azimuthally to afford one-dimensional (1D) scattering patterns as intensity ($I$) versus $q$.

The 1D scattering patterns were analyzed using a macro available from the NIST Center for Neutron Research (NCNR) for IGOR Pro (WaveMetrics, Inc.) data analysis software.[49] The background (*i.e.*, water and capillary scattering) was fit to a power law ($I(q) = A + Bq^{-n}$) and subtracted from the solution scattering data. The background-corrected traces obtained at 80 °C were fit to the form factor for a flexible cylinder with a disperse radius.[50,51]

**Cryogenic Transmission Electron Microscopy (cryo-TEM).** For cryo-TEM experiments, a solution of 0.75 mg/mL MC-*g*-PNIPAm with $\sigma$ = 0.03 was prepared and heated at 80 °C for 30 min prior to vitrification. Lacy carbon/formvar-coated copper TEM grids (Ted Pella, 300 mesh) were cleaned and hydrophilized using a PELCO easiGlow discharge cleaning system. Five microliters of solution were pipetted onto the TEM grid inside an FEI Vitrobot Mark IV vitrification system with the climate control set to 60 °C and 100% relative humidity. The sample was annealed in the chamber for 1 s before the grid was blotted for 1 s, with the instrument-defined blot force set to −1, equilibrated for 1 s, and plunge-frozen into liquid ethane cooled by liquid nitrogen. Samples were stored in liquid nitrogen prior to imaging. The grids were transferred under liquid nitrogen to a Gatan-626 single-tilt cryo-holder and imaged using an FEI Eagle charge-coupled device camera (2048 × 2048 pixels) on an FEI Tecnai G2 Spirit BioTWIN microscope operated at 120 kV. Images were obtained from multiple areas of the grids to determine if fibril formation occurred.

## RESULTS AND DISCUSSION

**Effect of PNIPAm Grafting Density.** To determine the effect of PNIPAm grafting on the chain conformations of MC in aqueous solution, a series of PNIPAm-grafted MC with seven different grafting densities ($\sigma$ = 0–0.11) were synthesized from allylated-MC and characterized by SLS and DLS at room temperature. In SLS experiments, the average scattered intensity is measured as a function of angle and concentration to probe dilute polymer solution interactions. The solvent intensity is subtracted, and the polymer Rayleigh ratio ($R_\theta$) is calculated for each angle with respect to a toluene standard: $R_\theta = R_{\theta,\text{toluene}}(I_{\text{solution}}(\theta) - I_{\text{solvent}}(\theta))/I_{\text{toluene}}(\theta)$. $R_\theta$ is the excess scattered intensity from the polymer and depends on the polymer weight average molecular weight ($M_w$), concentration ($c$), radius of gyration ($R_g$), and polymer–solvent interactions, characterized by the second virial coefficient ($A_2$). The Zimm equation defines the relationship[52]

$$\frac{Kc}{R_\theta} = \frac{1}{M_w}\left(1 + \frac{R_g^2 q^2}{3} + \ldots\right) + 2A_2 c + \ldots \quad (1)$$

where $K = 4\pi^2 n^2 (\partial n/\partial c)^2 \lambda_0^{-4} N_A^{-1}$ is the optical constant, $n$ is the solvent refractive index, $\partial n/\partial c$ is the refractive index increment, $\lambda_0$ is the laser wavelength in vacuum, and $N_A$ is Avogadro's number. Through Zimm analysis, $Kc/R_\theta$ is plotted versus $k'c + \sin^2(\theta/2)$ for each angle and concentration measured, where $k'$ is an arbitrary constant. Zimm plots for each PNIPAm grafting density are reported in Figure S4. Data for each angle were extrapolated to zero concentration, and the slope to the zero-concentration line determines $R_g$. Results for each concentration were extrapolated to zero angle, and the slope yielded $A_2$. The intercept from both extrapolations yields $1/M_w$. Table 1 lists values for $R_g$, $M_w$, and $A_2$ obtained for each

**Table 1. Solution Parameters of MC-*g*-PNIPAm Copolymers at Room Temperature**

| NMR $\sigma$ | SLS $\sigma$ | $R_g$ (nm) | $R_h$ (nm) | $M_w$ (kg/mol) | $A_2$ (mol cm$^3$/g$^2$) | $\chi_{eff}$ |
|---|---|---|---|---|---|---|
| 0 | 0 | 50 | 22 | 150 | 0.0012 | 0.46 |
| 0.007 | 0.016 | 52 | 19 | 188 | 0.0011 | 0.47 |
| 0.019 | 0.013 | 50 | 22 | 180 | 0.0015 | 0.46 |
| 0.028 | 0.028 | 56 | 23 | 218 | 0.0006 | 0.48 |
| 0.036 | 0.039 | 58 | 24 | 244 | 0.0011 | 0.47 |
| 0.084 | 0.044 | 70 | | 260 | 0.0096 | 0.25 |
| 0.105 | 0.055 | 79 | 22 | 283 | 0.0035 | 0.41 |

MC-*g*-PNIPAm copolymer. Both $R_g$ and $M_w$ increased monotonically with $\sigma$, while $A_2$ remained positive and relatively constant at low grafting densities; the increase in $R_g$ as a function of grafting density is shown in Figure 2. The increase

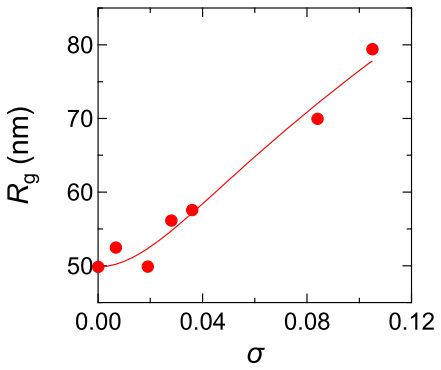


**Figure 2.** $R_g$ from Zimm plots of PNIPAm-grafted MC as a function of grafting density at room temperature. The solid curve is a fit to eq 3, with $R_{g,0}$ = 50 nm, $\alpha$ = 0.4 ± 9, and $\beta$ = 750 ± 150.

in $M_w$ from 150 to 283 kg/mol is caused by the PNIPAm grafts; the results were consistent with the NMR determination of $\sigma$ for low grafting densities but deviated somewhat at higher $\sigma$. For $\sigma$ = 0.084 and 0.105 by NMR, the $M_w$ should be 352 and 403 kg/mol, respectively. Instead, based on SLS, $M_w$ for these polymers are 260 and 283 kg/mol, which gives $\sigma$ = 0.044 and 0.055, respectively. This is about half the grafting density determined by NMR. The deviation in $M_w$ could be the result of incorrect estimates for $\partial n/\partial c$ or changes in concentration due to the filtration, though the former is more likely as the polymer size is much smaller than the pore size of the filters (0.45 $\mu$m).


https://doi.org/10.1021/acs.macromol.1c02206
Macromolecules 2022, 55, 550–558

Theory predicts that the free energy of a grafted coil is the sum of the stretching entropy and the excluded volume effects caused by the grafts and their interactions[22,23,53−57]

$$\frac{\Delta F}{k_B T} = \frac{3R_g^2}{2Na^2} + \frac{v_1 a^3 N^2}{R_g^3} + \frac{v_2 V^3 \sigma b N^2}{R_g^3} + \frac{v_3 R_m^3 (\sigma b N)^2}{R_g^3} \quad (2)$$

Here, $R_g$ is the copolymer radius of gyration, $N$ is the number of statistical segments of length $a$, $b$ is the number of anhydroglucose repeat units (AGUs) per statistical segment length, $v_1 a^3$ is the monomer-to-monomer excluded volume, $v_2 V^3$ is the graft-to-monomer excluded volume, $v_3 R_m{}^3$ is the graft-to-graft excluded volume, and $R_m{}^3$ is the volume of a graft. To determine the equilibrium size of a grafted coil, eq 2 is minimized with respect to $R_g$, which leads to

$$R_g = R_{g,0}\left(1 + \frac{v_2 V^3}{v_1 a^3} b\sigma + \frac{v_3 R_m^3}{v_1 a^3} b^2 \sigma^2\right)^{1/5} \sim R_{g,0}(1 + \alpha\sigma + \beta\sigma^2)^{1/5} \quad (3)$$

where $R_{g,0}$ is the radius of gyration of the ungrafted chain, $\alpha$ is a ratio of the graft−backbone interactions versus the backbone−backbone interactions, and $\beta$ is a ratio of the graft−graft interactions versus backbone−backbone interactions. The $R_g$ values obtained from light scattering were fit to eq 3 in Figure 2, with $\alpha$ and $\beta$ as fitting parameters (solid curve). The theory captured the experimental trend and gave $\alpha$ = 0.4 ± 9 and $\beta$ = 750 ± 150, suggesting that graft−graft interactions have more of an effect than graft−backbone interactions. Previously, Morozova et al.[22,23] used the same model to capture the effect of PEG grafts on MC coil dimensions, where for 0.8 kg/mol PEG grafts, $\alpha$ = 26 and $\beta \sim$ 0, and for 2 kg/mol PEG grafts, $\alpha$ = 22 and $\beta \sim$ 250. In contrast, PNIPAm-grafted MC had a higher $\beta$ value, presumably reflecting the increase in graft molecular weight to 3 kg/mol.

To understand how the chain flexibility changes with PNIPAm grafting, the Kratky−Porod wormlike chain model was numerically solved using the $R_g$ results to determine the persistence length ($l_p$)[58]

$$R_g^2 = \frac{1}{3} l_p L - l_p^2 + \frac{2 l_p^4}{L^2}\left(\exp\left(-\frac{L}{l_p}\right) - 1\right) + \frac{2 l_p^3}{L} \quad (4)$$

where $L$ is the fixed contour length, estimated as ∼560 nm based on the MC average molecular weight and a monomer length of 0.7 nm.[19] $l_p$ increased with increasing grafting density, as shown in Figure 3, which can be attributed to the polymer becoming less flexible due to increased excluded volume interactions driven by the grafted chains. Relative to the PEG-grafted MC,[22,23] the persistence length of MC-*g*-PNIPAm increased to a greater extent at low grafting densities. For $\sigma$ = 0.11, $l_p$ = 42 nm, whereas for 0.8 kg/mol PEG grafts, $l_p \sim$ 20 nm at $\sigma \sim$ 0.12, and for 2 kg/mol PEG grafts, $l_p \sim$ 30 nm at $\sigma \sim$ 0.15. The larger increase in $l_p$ for 3 kg/mol PNIPAm grafts also likely results from the increased graft−graft excluded volume interactions (as shown by the larger $\beta$ value), which cause the chain to form a more extended conformation for a given number density of grafts. This is also consistent with theories where increasing graft length increases local stiffness.[55,59,60]

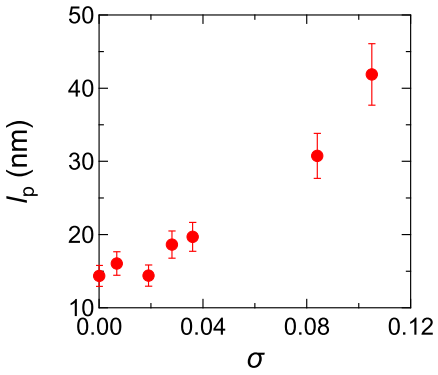


**Figure 3.** Calculated persistence length of MC-*g*-PNIPAm as a function of grafting density. Error bars indicate an estimated ± 10% uncertainty.

To gain an understanding of the effects of PNIPAm grafting on the polymer interactions with water, we consider the second virial coefficient ($A_2$). At room temperature, $A_2$ remained relatively constant at low grafting densities and increases for the largest two grafting densities. We can estimate an effective Flory−Huggins interaction parameter ($\chi_{eff}$) between water and the grafted polymers at room temperature as a measure of the polymer−polymer interactions relative to the polymer−solvent interactions using[61]

$$A_2 = \left(\frac{1}{2} - \chi_{eff}\right)\frac{\bar{V}_p^2}{M_0{}^2 \bar{V}_s} \quad (5)$$

where $\bar{V}_s$ is the solvent molar volume (18 cm$^3$/mol), $\bar{V}_p$ is the polymer repeat unit molar volume (volume-fraction-weighted average of MC (140 cm$^3$/mol) and PNIPAm (103 cm$^3$/mol)), and $M_0$ is the repeat unit molecular weight (volume-fraction-weighted average of MC (187 g/mol) and PNIPAm (113 g/mol)). The $\chi_{eff}$ values (Table 1) remained constant at around 0.47 for low grafting densities and decreased modestly to 0.41 for the highest grafting density, $\sigma$ = 0.11. This suggests that solvent quality may improve slightly with increased grafting density. The $\chi_{eff}$ value for $\sigma$ = 0.08 appeared to be an outlier with $\chi_{eff}$ = 0.25.

Dynamic light scattering (DLS) affords another measure of polymer size in solution and also provides insight into the size distribution. With increasing grafting density, the hydrodynamic radius ($R_h$) remained relatively constant (Figure 4a), in contrast to previous work with PEG-grafted MC where $R_h$ increased with $\sigma$.[22] Combining the DLS and SLS results, we can assess the coil configuration in solution using the shape factor $\rho = R_g/R_h$, which varies from about 1.7 for high-molecular-weight disperse ($Đ > 2$) Gaussian coils to about 2 for disperse chains in a good solvent.[62,63] For MC-*g*-PNIPAm, $R_g/R_h$ remained around 2−2.5 for $\sigma < 0.04$ (Figure 4b), suggesting that the polymer chains are semiflexible coils in solution.

**Effect of Temperature.** To determine the effect of temperature on PNIPAm-grafted MC, two samples (ungrafted MC and MC-*g*-PNIPAm with $\sigma$ = 0.03) were chosen, and changes in coil dimensions upon heating were examined using SLS, DLS, SAXS, and cryo-TEM. Each sample was characterized at four to five different temperatures. SLS was performed after annealing the solutions for 30 min at each temperature to keep the thermal history of the samples consistent. Zimm plot analysis was used to determine $R_g$,


https://doi.org/10.1021/acs.macromol.1c02206
Macromolecules 2022, 55, 550−558

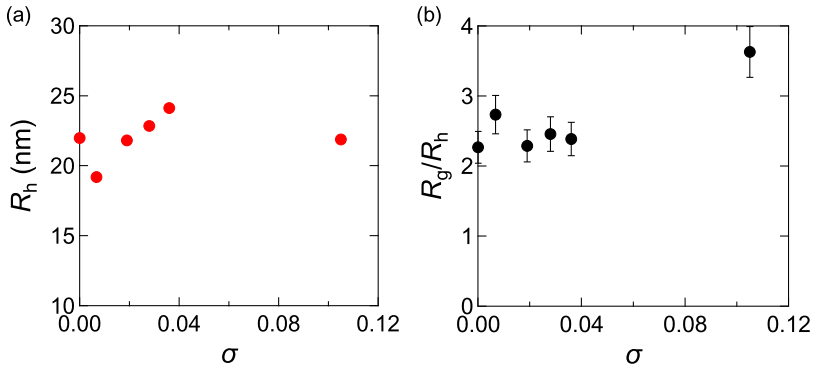


**Figure 4.** Summary of DLS data for 1 mg/mL solutions of PNIPAm-grafted MC at room temperature. (a) $R_h$ as a function of grafting density. (b) Shape factor $R_g/R_h$ remained relatively constant around 2−2.5 for low grafting densities but increased at the highest grafting density. Error bars indicate an estimated ± 10% uncertainty.

**Table 2. Solution Parameters of MC and MC-*g*-PNIPAm with $\sigma$ = 0.03 as a Function of Temperature**

| | $R_g$ (nm) | | $R_h$ (nm) | | $M_w$ (kg/mol) | | $A_2$ (mol cm$^3$/g$^2$) | |
|---|---|---|---|---|---|---|---|---|
| $T$ (°C) | $\sigma$ = 0 | $\sigma$ = 0.03 | $\sigma$ = 0 | $\sigma$ = 0.03 | $\sigma$ = 0 | $\sigma$ = 0.03 | $\sigma$ = 0 | $\sigma$ = 0.03 |
| 23 | 50 | 56 | 22 | 23 | 150 | 218 | 0.0012 | 0.0006 |
| 30 | 49 | | 22 | 23 | 138 | | 0.0009 | |
| 35 | 47 | 51 | 22 | 23 | 144 | 165 | 0.0010 | 0.0002 |
| 40 | 46 | | 23 | 24 | 132 | | 0.0007 | |
| 50 | 43 | 50 | 27 | 25 | 121 | 145 | −0.0010 | 0.0001 |
| 55 | | 44 | | | | 127 | | −0.0009 |

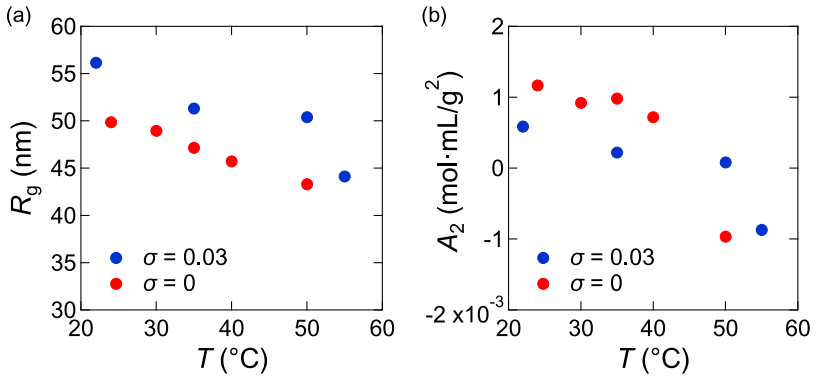


**Figure 5.** Summary of SLS data for MC (red) and MC-*g*-PNIPAm with $\sigma$ = 0.03 (blue) as a function of temperature. (a) $R_g$ decreases for both polymers with increasing temperature. (b) $A_2$ becomes negative at a higher temperature for MC-*g*-PNIPAm than for MC, indicating an increase in the theta temperature upon grafting.

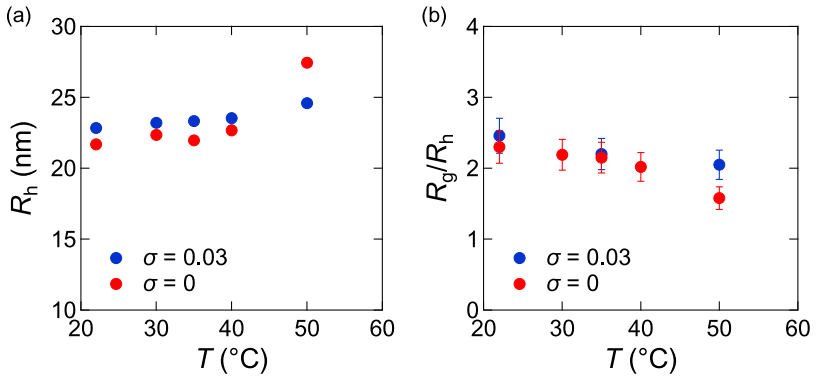


**Figure 6.** Summary of DLS data for 1 mg/mL solutions of MC (red) and MC-*g*-PNIPAm with $\sigma$ = 0.03 (blue) as a function of temperature. (a) $R_h$ remains relatively constant for both polymers with increasing temperature until 50 °C, where it increased for MC. (b) Shape factor $R_g/R_h$ remained relatively constant around 2−2.5 for both polymers with increasing temperature until 50 °C, where it decreased for MC. Error bars indicate an estimated ± 10% uncertainty.



https://doi.org/10.1021/acs.macromol.1c02206
*Macromolecules* 2022, 55, 550−558

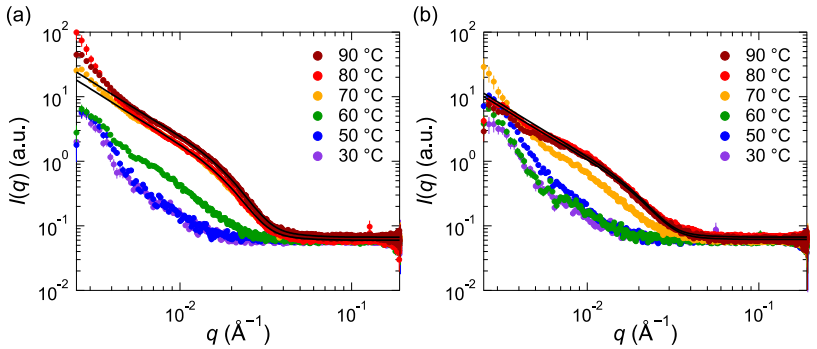


**Figure 7.** SAXS data as a function of temperature for 0.75 mg/mL solutions of (a) MC and (b) MC-*g*-PNIPAm with $\sigma$ = 0.03. The sample was annealed at each temperature for 30 min before measurement. Fibrils start to form at a higher temperature for PNIPAm-grafted MC (70 °C) compared to that for MC (60 °C). Black curves are fits to a semiflexible cylinder model.

apparent $M_w$, and $A_2$ for both polymers at each temperature (Figures S5 and S6). The results are listed in Table 2. As shown in Figure 5a, the $R_g$ for both polymers decreased upon heating, though MC-*g*-PNIPAm decreased to a larger extent from 56 nm at room temperature to 44 nm at 55 °C. A temperature-independent $\partial n/\partial c$ was assumed, which could partly account for the apparent $M_w$ decreases with temperature, as the chemical structure did not change with heating.

For MC, $A_2$ decreased upon heating and becomes negative between 40 and 50 °C (Figure 5b). This is consistent with previous work on MC, which determined that the theta temperature ($T_\theta$) for MC is 48 ± 2 °C.[14] For MC-*g*-PNIPAm, $T_\theta$ apparently increased as $A_2$ only becomes negative at 55 °C. This result was unexpected as the graft polymers consist of components that should be self-attracting as $T$ increases. However, the increase in $T_\theta$ result suggests that the net interactions between PNIPAm and MC are unfavorable, which forces the polymer to remain in solution to maintain separation between the backbone and the grafts. Similar results have been shown previously for other copolymer systems.[64,65] This behavior is also analogous to the well-known partial miscibility of poly(styrene-*stat*-acrylonitrile) (SAN) and poly(methyl methacrylate) (PMMA), even though PS/PMMA and PAN/PMMA are immiscible pairs; this arises simply from the greater $\chi$ for PS/PAN than for the other two pairs.

Multiangle DLS was performed on the same two polymers at scattering angles from 50° to 130° after annealing the samples for 30 min at each temperature. Upon heating, $R_h$ remained relatively constant for both polymers until 50 °C where it increased from ∼22 to 27 nm for MC (Figure 6a). This increase above $T_\theta$ suggests that MC is beginning to aggregate as the net interactions with water become unfavorable. Aggregation of MC was confirmed upon annealing the polymers at 50 °C for over 24 h (Figure S7). The $R_h$ for MC increased from 27 nm to 44 nm during this period, while that of MC-*g*-PNIPAm remained unchanged. MC is known to aggregate slowly over time under these conditions, although the time required for aggregation depends on concentration and on the annealing temperature.[14] MC can also aggregate below $T_\theta$, although it can take days to do so at 40 °C.[14] The coil configuration was also assessed using the shape factor, $R_g/R_h$. Upon heating, $R_g/R_h$ remained around 2−2.5 for both polymers until 50 °C, where it decreased slightly for the ungrafted MC (Figure 6b). This indicates that both polymers remain semiflexible coils in solution upon heating, though the decrease for MC at 50 °C can be attributed to the shift from a good solvent to a poor solvent.

Small-angle X-ray scattering (SAXS) was used to determine whether fibril formation still occurs in solutions of MC-*g*-PNIPAm. The samples were heated, and the structure was examined as a function of temperature, annealing for 30 min before each measurement. The SAXS results, plotted as intensity ($I$) versus $q$, are shown in Figure 7. For MC (Figure 7a), the fibrillar shoulder started to appear at 60 °C, which agrees with results from previous publications.[12,15−18,23,66] Comparatively, the fibrillar shoulder did not appear until 70 °C for MC-*g*-PNIPAm (Figure 7b), which is qualitatively consistent with the increase in $T_\theta$ with grafting. The SAXS data at 80 and 90 °C were fit to a flexible cylinder model as in previous publications,[15−18,23,66] showing that fibril radius decreased slightly with grafting, from 8.3 nm in MC to 7.8 nm in MC-*g*-PNIPAm with $\sigma$ = 0.03, which is opposite to the trend seen in previous work on PEG-grafted MC.[23] Further investigations are needed to determine if the decrease in fibril radius persists over a wider range of grafting densities.

To characterize changes in the structure of the fibrils, cryogenic transmission electron microscopy was used to directly image the fibrils formed in MC-*g*-PNIPAm. As shown in Figure 8, cryo-TEM confirmed that fibril formation occurs in a 0.75 mg/mL solution of PNIPAm-grafted MC with $\sigma$ = 0.03 at 80 °C. The fibrils were relatively short, with lengths ranging from 20 to 200 nm, whereas MC of the same molecular weight typically has much longer fibrils.[17] Some aggregates can be seen with similar contrast as the fibrillar structures, which is similar to the change in fibrillar structure seen in PEG-grafted MC where fibrils become increasingly shorter with increased grafting density until no fibrils are formed.[23] MC fibrils are known to have both semicrystalline and amorphous domains,[18] and the grafts are unlikely to participate in the formation of the semicrystalline regions. Thus, one possible explanation for the decrease in fibril length is the disruption of formation of the semicrystalline domains with increased grafting density. Further investigation into the fibrillar dimensions and subfibrillar structure at higher grafting densities is needed to be more conclusive.

## SUMMARY

Upon heating, aqueous solutions of MC will gel as fibril formation occurs. The self-assembly of chains into fibrils and modification of the fibrillar structure is of particular interest. Our results showed that the addition of PNIPAm grafts onto the MC backbone causes an increase in the persistence length and radius of gyration of the polymer, yet the polymers


https://doi.org/10.1021/acs.macromol.1c02206
Macromolecules 2022, 55, 550−558

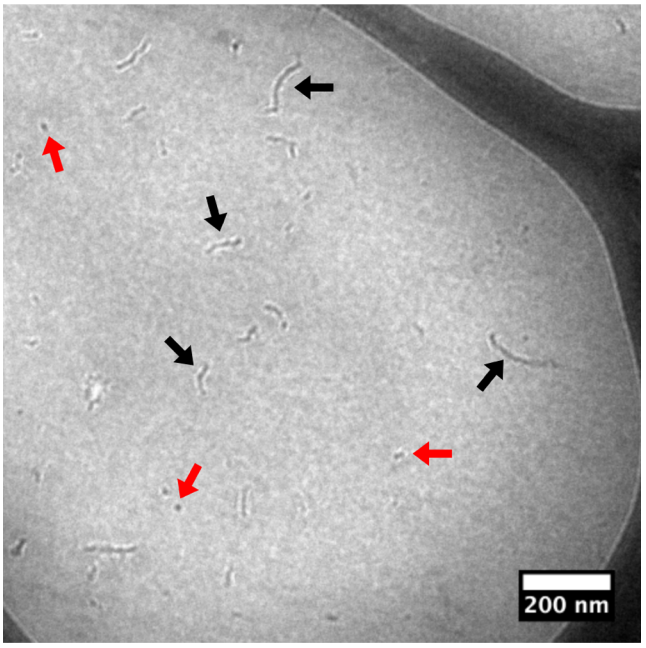


**Figure 8.** Cryo-TEM of 0.75 mg/mL MC-*g*-PNIPAm with $\sigma$ = 0.03 shows that fibril formation still occurred at a higher temperature. The sample was vitrified from 80 °C after 30 min annealing. Black arrows indicate short fibrils, and red arrows indicate aggregates.

remained semiflexible coils at lower grafting densities. These results were similar to previous work on grafting PEG onto MC, although the persistence length increased to a larger extent for the PNIPAm-grafted MC due to increased excluded volume interactions. Additionally, unfavorable interactions between MC and PNIPAm slightly elevated the theta temperature of MC after grafting, even though PNIPAm itself has a lower LCST than MC. Fibril formation still occurred for MC-*g*-PNIPAm, but the length of the fibrils was reduced significantly, similar to what has been found with PEG-grafted MC.

## ■ ASSOCIATED CONTENT

### Supporting Information

The Supporting Information is available free of charge at https://pubs.acs.org/doi/10.1021/acs.macromol.1c02206.

Synthetic details for grafting of PNIPAm to MC and associated $^1$H NMR spectra; REPES analysis of dynamic light scattering data for MC-*g*-PNIPAm as a function of grafting density; Zimm plots from light scattering data for MC-*g*-PNIPAm as a function of grating density at room temperature and as a function of temperature; and time evolution of hydrodynamic radius for MC and for MC-g-PNIPAm while annealing at 50 °C (PDF)

## ■ AUTHOR INFORMATION


### Corresponding Authors

**Frank S. Bates** − *Department of Chemical Engineering and Materials Science, University of Minnesota, Minneapolis, Minnesota 55455, United States;* orcid.org/0000-0003-3977-1278; Email: bates001@umn.edu

**Timothy P. Lodge** − *Department of Chemical Engineering and Materials Science, University of Minnesota, Minneapolis, Minnesota 55455, United States; Department of Chemistry, University of Minnesota, Minneapolis, Minnesota 55455, United States;* orcid.org/0000-0001-5916-8834; Email: lodge@umn.edu

### Authors

**McKenzie L. Coughlin** − *Department of Chemical Engineering and Materials Science, University of Minnesota, Minneapolis, Minnesota 55455, United States;* orcid.org/0000-0001-9047-3319

**Jerrick Edmund** − *Department of Chemical Engineering and Materials Science, University of Minnesota, Minneapolis, Minnesota 55455, United States*

Complete contact information is available at: https://pubs.acs.org/10.1021/acs.macromol.1c02206


### Notes

The authors declare no competing financial interest.

## ■ ACKNOWLEDGMENTS

This work was supported by the National Science Foundation through the University of Minnesota MRSEC under Award Numbers DMR-1420013 and DMR-02011401, as well as by the National Science Foundation Graduate Research Fellowship Program (M.L.C.) under Grant Numbers 00039202 and 00074041. The authors thank the Dow Chemical Company for generously providing the MC samples. The SAXS measurements were taken at the DuPont-Northwestern-Dow Collaborative Access Team (DND-CAT) located at Sector 5 of the Advanced Photon Source (APS). DND-CAT was supported by Northwestern University, E.I. DuPont de Nemours & Co., and the Dow Chemical Company. This research used resources of the Advanced Photon Source, a U.S. Department of Energy (DOE) Office of Science User Facility operated for the DOE Office of Science by Argonne National Laboratory under Contract No. DE-AC02-06CH11357. Data were collected using an instrument funded by the National Science Foundation under Award Number 0960140. The cryo-TEM images were collected at the Characterization Facility, University of Minnesota, which receives partial support from NSF through the MRSEC program. The authors thank Dr. Svetlana Morozova and Dr. S. Piril Ertem for helpful discussions regarding synthesis and light scattering experiments, as well as Dr. Peter W. Schmidt for insightful discussions regarding X-ray characterization and cryo-TEM experiments.

## ■ REFERENCES

(1) Nasatto, P. L.; Pignon, F.; Silveira, J. L. M.; Duarte, M. E. R.; Noseda, M. D.; Rinaudo, M. Methylcellulose, a Cellulose Derivative with Original Physical Properties and Extended Applications. *Polymers* **2015**, *7*, 777−803.

(2) Sarkar, N. Thermal Gelation Properties of Methyl and Hydroxypropyl Methylcellulose. *J. Appl. Polym. Sci.* **1979**, *24*, 1073−1087.

(3) Haque, A.; Morris, E. R. Thermogelation of Methylcellulose. Part I: Molecular Structures and Processes. *Carbohydr. Polym.* **1993**, *22*, 161−173.

(4) Takahashi, M.; Shimazaki, M.; Yamamoto, J. Thermoreversible Gelation and Phase Separation in Aqueous Methyl Cellulose Solutions. *J. Polym. Sci., Part B: Polym. Phys.* **2001**, *39*, 91−100.

(5) Chevillard, C.; Axelos, M. A. V. Phase Separation of Aqueous Solution of Methylcellulose. *Colloid Polym. Sci.* **1997**, *275*, 537−545.

(6) Fairclough, J. P. A.; Yu, H.; Kelly, O.; Ryan, A. J.; Sammler, R. L.; Radler, M. Interplay between Gelation and Phase Separation in

Aqueous Solutions of Methylcellulose and Hydroxypropylmethylcellulose. *Langmuir* **2012**, *28*, 10551−10557.
(7) Kobayashi, K.; Huang, C. I.; Lodge, T. P. Thermoreversible Gelation of Aqueous Methylcellulose Solutions. *Macromolecules* **1999**, *32*, 7070−7077.
(8) Chatterjee, T.; Nakatani, A. I.; Adden, R.; Brackhagen, M.; Redwine, D.; Shen, H.; Li, Y.; Wilson, T.; Sammler, R. L. Structure and Properties of Aqueous Methylcellulose Gels by Small-Angle Neutron Scattering. *Biomacromolecules* **2012**, *13*, 3355−3369.
(9) Desbrières, J.; Hirrien, M.; Ross-Murphy, S. B. Thermogelation of Methylcellulose: Rheological Considerations. *Polymer* **2000**, *41*, 2451−2461.
(10) Heymann, E. Studies on Sol-Gel Transformations I. The Inverse Sol-Gel Transformation of Methylcellulose in Water. *Trans. Faraday Soc.* **1935**, *31*, 846.
(11) Nishinari, K.; Hofmann, K. E.; Moritaka, H.; Kohyama, K.; Nishinari, N. Gel-Sol Transition of Methylcellulose. *Macromol. Chem. Phys.* **1997**, *198*, 1217−1226.
(12) Coughlin, M. L.; Liberman, L.; Ertem, S. P.; Edmund, J.; Bates, F. S.; Lodge, T. P. Methyl Cellulose Solutions and Gels: Fibril Formation and Gelation Properties. *Prog. Polym. Sci.* **2021**, *112*, No. 101324.
(13) Arvidson, S. A.; Lott, J. R.; McAllister, J. W.; Zhang, J.; Bates, F. S.; Lodge, T. P.; Sammler, R. L.; Li, Y.; Brackhagen, M. Interplay of Phase Separation and Thermoreversible Gelation in Aqueous Methylcellulose Solutions. *Macromolecules* **2013**, *46*, 300−309.
(14) McAllister, J. W.; Schmidt, P. W.; Dorfman, K. D.; Lodge, T. P.; Bates, F. S. Thermodynamics of Aqueous Methylcellulose Solutions. *Macromolecules* **2015**, *48*, 7205−7215.
(15) Lott, J. R.; McAllister, J. W.; Arvidson, S. A.; Bates, F. S.; Lodge, T. P. Fibrillar Structure of Methylcellulose Hydrogels. *Biomacromolecules* **2013**, *14*, 2484−2488.
(16) Lott, J. R.; McAllister, J. W.; Wasbrough, M.; Sammler, R. L.; Bates, F. S.; Lodge, T. P. Fibrillar Structure in Aqueous Methylcellulose Solutions and Gels. *Macromolecules* **2013**, *46*, 9760−9771.
(17) Schmidt, P. W.; Morozova, S.; Owens, P. M.; Adden, R.; Li, Y.; Bates, F. S.; Lodge, T. P. Molecular Weight Dependence of Methylcellulose Fibrillar Networks. *Macromolecules* **2018**, *51*, 7767−7775.
(18) Schmidt, P. W.; Morozova, S.; Ertem, S. P.; Coughlin, M. L.; Davidovich, I.; Talmon, Y.; Reineke, T. M.; Bates, F. S.; Lodge, T. P. Internal Structure of Methylcellulose Fibrils. *Macromolecules* **2020**, *53*, 398−405.
(19) Bodvik, R.; Dedinaite, A.; Karlson, L.; Bergström, M.; Bäverbäck, P.; Pedersen, J. S.; Edwards, K.; Karlsson, G.; Varga, I.; Claesson, P. M. Aggregation and Network Formation of Aqueous Methylcellulose and Hydroxypropylmethylcellulose Solutions. *Colloids Surf., A* **2010**, *354*, 162−171.
(20) McAllister, J. W.; Lott, J. R.; Schmidt, P. W.; Sammler, R. L.; Bates, F. S.; Lodge, T. P. Linear and Nonlinear Rheological Behavior of Fibrillar Methylcellulose Hydrogels. *ACS Macro Lett.* **2015**, *4*, 538−542.
(21) Liberman, L.; Schmidt, P. W.; Coughlin, M. L.; Ya'akobi, A. M.; Davidovich, I.; Edmund, J.; Ertem, S. P.; Morozova, S.; Talmon, Y.; Bates, F. S.; et al. Salt-Dependent Structure in Methylcellulose Fibrillar Gels. *Macromolecules* **2021**, *54*, 2090−2100.
(22) Morozova, S.; Lodge, T. P. Conformation of Methylcellulose as a Function of Poly(Ethylene Glycol) Graft Density. *ACS Macro Lett.* **2017**, *6*, 1274−1279.
(23) Morozova, S.; Schmidt, P. W.; Bates, F. S.; Lodge, T. P. Effect of Poly(Ethylene Glycol) Grafting Density on Methylcellulose Fibril Formation. *Macromolecules* **2018**, *51*, 9413−9421.
(24) Sethuraman, V.; Dorfman, K. D. Origins of the Suppression of Fibril Formation in Grafted Methylcellulose Solutions. *Phys. Rev. Mater.* **2020**, *4*, No. 085601.
(25) Roy, D.; Semsarilar, M.; Guthrie, J. T.; Perrier, S. Cellulose Modification by Polymer Grafting: A Review. *Chem. Soc. Rev.* **2009**, *38*, 2046.
(26) Zhang, J.; Li, T.; Mannion, A. M.; Schneiderman, D. K.; Hillmyer, M. A.; Bates, F. S. Tough and Sustainable Graft Block Copolymer Thermoplastics. *ACS Macro Lett.* **2016**, *5*, 407−412.
(27) Hu, H.; You, J.; Gan, W.; Zhou, J.; Zhang, L. Synthesis of Allyl Cellulose in NaOH/Urea Aqueous Solutions and Its Thiol−Ene Click Reactions. *Polym. Chem.* **2015**, *6*, 3543−3548.
(28) Zheng, J.; Jung, S.; Schmidt, P. W.; Lodge, T. P.; Reineke, T. M. 2-Hydroxyethylcellulose and Amphiphilic Block Polymer Conjugates Form Mechanically Tunable and Nonswellable Hydrogels. *ACS Macro Lett.* **2017**, *6*, 145−149.
(29) Wohlhauser, S.; Delepierre, G.; Labet, M.; Morandi, G.; Thielemans, W.; Weder, C.; Zoppe, J. O. Grafting Polymers from Cellulose Nanocrystals: Synthesis, Properties, and Applications. *Macromolecules* **2018**, *51*, 6157−6189.
(30) Huang, J.-L.; Li, C.-J.; Gray, D. G. Functionalization of Cellulose Nanocrystal Films via "Thiol−Ene" Click Reaction. *RSC Adv.* **2014**, *4*, 6965.
(31) Heskins, M.; Guillet, J. E. Solution Properties of Poly(N-Isopropylacrylamide). *J. Macromol. Sci., Part A* **1968**, *2*, 1441−1455.
(32) Fujishige, S.; Kubota, K.; Ando, I. Phase Transition of Aqueous Solutions of Poly(N-Isopropylacrylamide) and Poly(N-Isopropylmethacrylamide). *J. Phys. Chem. A* **1989**, *93*, 3311−3313.
(33) Kubota, K.; Fujishige, S.; Ando, I. Single-Chain Transition of Poly(N-Isopropylacrylamide) in Water. *J. Phys. Chem. A* **1990**, *94*, 5154−5158.
(34) Kubota, K.; Fujishige, S.; Ando, I. Solution Properties of Poly(N-Isopropylacrylamide) in Water. *Polym. J.* **1990**, *22*, 15−20.
(35) Schild, H. G. Poly(N-Isopropylacrylamide): Experiment, Theory and Application. *Prog. Polym. Sci.* **1992**, *17*, 163−249.
(36) Wu, C.; Zhou, S. Laser Light Scattering Study of the Phase Transition of Poly(N-Isopropylacrylamide) in Water. I: Single Chain. *Macromolecules* **1995**, *28*, 8381−8387.
(37) Zeng, F.; Zheng, X.; Tong, Z. Network Formation in Poly(N-Isopropyl Acrylamide)/Water Solutions during Phase Separation. *Polymer* **1998**, *39*, 1249−1251.
(38) Zeng, F.; Liu, X.; Tong, Z.; Yang, Y.; Wu, S. Thermal Reversible Gelation during Phase Separation of Poly(N-Isopropyl Acrylamide)/Water Solution. *Sci. China, Ser. B: Chem.* **2000**, *43*, 428−434.
(39) Halperin, A.; Kröger, M.; Winnik, F. M. Poly(N -Isopropylacrylamide) Phase Diagrams: Fifty Years of Research. *Angew. Chem., Int. Ed.* **2015**, *54*, 15342−15367.
(40) Patenaude, M.; Hoare, T. Injectable, Mixed Natural-Synthetic Polymer Hydrogels with Modular Properties. *Biomacromolecules* **2012**, *13*, 369−378.
(41) Conova, L.; Vernengo, J.; Jin, Y.; Himes, B. T.; Neuhuber, B.; Fischer, I.; Lowman, A.; Vernengo, J.; Jin, Y.; Himes, B. T.; et al. A Pilot Study of Poly(N-Isopropylacrylamide)-g-Polyethylene Glycol and Poly(N-Isopropylacrylamide)-g-Methylcellulose Branched Copolymers as Injectable Scaffolds for Local Delivery of Neurotrophins and Cellular Transplants into the Injured Spinal Cord. *J. Neurosurg.* **2011**, *15*, 594−604.
(42) Liu, W.; Zhang, B.; Lu, W. W.; Li, X.; Zhu, D.; De Yao, K.; Wang, Q.; Zhao, C.; Wang, C. A Rapid Temperature-Responsive Sol−Gel Reversible Poly(N-Isopropylacrylamide)-g-Methylcellulose Copolymer Hydrogel. *Biomaterials* **2004**, *25*, 3005−3012.
(43) Sá-Lima, H.; Tuzlakoglu, K.; Mano, J. F.; Reis, R. L. Thermoresponsive Poly(N-Isopropylacrylamide)-g-Methylcellulose Hydrogel as a Three-Dimensional Extracellular Matrix for Cartilage-Engineered Applications. *J. Biomed. Mater. Res. Part A* **2011**, *98A*, 596−603.
(44) Ifuku, S.; Kadla, J. F. Preparation of a Thermosensitive Highly Regioselective Cellulose/ N -Isopropylacrylamide Copolymer through Atom Transfer Radical Polymerization. *Biomacromolecules* **2008**, *9*, 3308−3313.
(45) Wu, H. Correlations between the Rayleigh Ratio and the Wavelength for Toluene and Benzene. *Chem. Phys.* **2010**, *367*, 44−47.
(46) Dynamic Light Scattering: The Method and Some Applications. In *Monographs on the Physics and Chemistry of Materials*;


https://doi.org/10.1021/acs.macromol.1c02206
*Macromolecules* 2022, 55, 550−558

Brown, W., Eds.; Clarendon Press; Oxford University Press: Oxford (England); New York, 1993; Vol. *49*.
(47) Schärtl, W. *Light Scattering from Polymer Solutions and Nanoparticle Dispersions*; Springer Laboratory, Springer: Berlin Heidelberg, 2007.
(48) Jakeš, J. Regularized Positive Exponential Sum (REPES) Program - A Way of Inverting Laplace Transform Data Obtained by Dynamic Light Scattering. *Collect. Czech. Chem. Commun.* **1995**, *60*, 1781−1797.
(49) Kline, S. R. Reduction and Analysis of SANS and USANS Data Using IGOR Pro. *J. Appl. Crystallogr.* **2006**, *39*, 895−900.
(50) Pedersen, J. S.; Schurtenberger, P. Scattering Functions of Semiflexible Polymers with and without Excluded Volume Effects. *Macromolecules* **1996**, *29*, 7602−7612.
(51) Chen, W. R.; Butler, P. D.; Magid, L. J. Incorporating Intermicellar Interactions in the Fitting of SANS Data from Cationic Wormlike Micelles. *Langmuir* **2006**, *22*, 6539−6548.
(52) Zimm, B. H. Apparatus and Methods for Measurement and Interpretation of the Angular Variation of Light Scattering; Preliminary Results on Polystyrene Solutions. *J. Chem. Phys.* **1948**, *16*, 1099−1116.
(53) Fredrickson, G. H. Surfactant-Induced Lyotropic Behavior of Flexible Polymer Solutions. *Macromolecules* **1993**, *26*, 2825−2831.
(54) Hsu, H.-P.; Paul, W.; Binder, K. Polymer Chain Stiffness vs. Excluded Volume: A Monte Carlo Study of the Crossover towards the Worm-like Chain Model. *Europhys. Lett.* **2010**, *92*, 28003.
(55) Hsu, H.-P.; Paul, W.; Binder, K. Understanding the Multiple Length Scales Describing the Structure of Bottle-Brush Polymers by Monte Carlo Simulation Methods. *Macromol. Theory Simul.* **2011**, *20*, 510−525.
(56) Rouault, Y.; Borisov, O. V. Comb-Branched Polymers: Monte Carlo Simulation and Scaling. *Macromolecules* **1996**, *29*, 2605−2611.
(57) Borisov, O. V.; Zhulina, E. B. Amphiphilic Graft Copolymer in a Selective Solvent: Intramolecular Structures and Conformational Transitions. *Macromolecules* **2005**, *38*, 2506−2514.
(58) Hiemenz, P. C.; Lodge, T. P. *Polymer Chemistry*, 2nd ed.; CRC Press, 2007.
(59) Fischer, K.; Schmidt, M. Solvent-Induced Length Variation of Cylindrical Brushes. *Macromol. Rapid Commun.* **2001**, *22*, 787−791.
(60) Sheiko, S. S.; Sumerlin, B. S.; Matyjaszewski, K. Cylindrical Molecular Brushes: Synthesis, Characterization, and Properties. *Prog. Polym. Sci.* **2008**, *33*, 759−785.
(61) Flory, P. J. *Principles of Polymer Chemistry*; Cornell University Press: Ithaca, NY, 1953.
(62) Franken, I.; Burchard, W. Application of the Cascade Theory to Calculation of Particle Scattering Factors of Polydisperse Systems of Stiff Chains. *Macromolecules* **1973**, *6*, 848−855.
(63) Burchard, W. Static and Dynamic Light Scattering from Branched Polymers and Biopolymers. *Adv. Polym. Sci.* **1983**, *48*, 1−124.
(64) Stockmayer, W. H. Problems of the Statistical Thermodynamics of Dilute Polymer Solutions. *Makromol. Chemie* **1960**, *35*, 54−74.
(65) Burchard, W.; Schmidt, M.; Stockmayer, W. H. Information on Polydispersity and Branching from Combined Quasi-Elastic and Integrated Scattering. *Macromolecules* **1980**, *13*, 1265−1272.
(66) Morozova, S. Methylcellulose Fibrils: A Mini Review. *Polym. Int.* **2020**, *69*, 125−130.


https://doi.org/10.1021/acs.macromol.1c02206
*Macromolecules* 2022, 55, 550−558